Optical detection of spin transport in non-magnetic metals

F. Fohr, S. Kaltenborn, J. Hamrle,* H. Schultheiß,† A. A. Serga, H. C. Schneider, and B. Hillebrands
Fachbereich Physik and Forschungszentrum OPTIMAS,
Technische Universität Kaiserslautern, D-67663 Kaiserslautern, Germany

Y. Fukuma, L. Wang, and Y. Otani
ASI, RIKEN, 2-1 Hirosawa, Wako 351-0198, and ISSP,
University of Tokyo, 5-15-5 Kashiwanoha, Kashiwa 277-8581, Japan.
(Dated: November 23, 2010)

We determine the dynamic magnetization induced in non-magnetic metal wedges composed of silver, copper and platinum by means of Brillouin light scattering (BLS) microscopy. The magnetization is transferred from a ferromagnetic $Ni_{80}Fe_{20}$ layer to the metal wedge via the spin pumping effect. The spin pumping efficiency can be controlled by adding an insulating but transparent interlayer between the magnetic and non-magnetic layer. By comparing the experimental results to a dynamical macroscopic spin-transport model we determine the transverse relaxation time of the pumped spin current which is much smaller than the longitudinal relaxation time.

Spin current injection from a magnetic to a non-magnetic material is an important and central issue of magneto-electronics [1, 2]. There are several ways to realize such an injection. Spin currents can be generated by spin polarized charge currents [3], the spin Hall effect [4], or spin pumping [5, 6]. The spin accumulation in the non-magnet can be detected indirectly by an increased damping in the injection layer [6, 7] or it can be probed by the conversion of spin current into voltage in a lateral spin valve [8, 9] or via the inverse spin Hall effect [10–12].

A direct imaging of the spin polarization in a non-magnetic metal is only possible using non-contact techniques. For instance, the spin polarization was mapped in a ferromagnet/semiconductor system by exploiting the connection of the spin polarization with the polarization of the probe laser light [13]. In metals, spin accumulation occurs only in the vicinity of the Fermi level (in the order of tens of μeV), making the observation of the spin accumulation difficult using techniques such as XMCD microscopy [14].

In the case of the spin pumping effect, the injected spin current is proportional to the cross product of the magnetization and its first time derivative and can be separated into a static (or longitudinal) component parallel and a dynamic (or transverse) component perpendicular to the external field. In this paper we demonstrate that the dynamic component can be observed directly by means of Brillouin light scattering (BLS) microscopy in a non-magnetic material.

We detect the spin polarization in a metal wedge grown on top of a ferromagnetic layer (see Fig. 1). Light from a laser is focussed on the surface of the wedge and the inelastically scattered light is collected as a function of the local wedge thickness. This light originates from the non-magnetic layer due to inelastic scattering from the spin polarization as well as from the magnetic layer below the wedge as long as the accumulated optical path length is smaller, or at least comparable to the optical absorption length. The magnetic layer is excited externally by the RF field of a coplanar waveguide (CPW) near the ferromagnetic resonance frequency, and generates the spin polarization in the wedge layer via the spin pumping effect.

The CPW is prepared by means of maskless laser photolithography on an oxidized silicon substrate. It consists of a 300 nm gold layer with a signal line (S) of 20 μm width separated from the ground planes (G) by a 10 μm wide gap. A microwave current is applied to the CPW and generates an oscillating magnetic field in y-direction using a coordinate system as defined in Fig. 1. To reach high microwave power in a wide frequency band and to prevent reflections, the microwave current is terminated by a load at the end of the CPW with impedance matching. On the CPW signal line a multilayer structure is deposited by electron beam evaporation.

The multilayer has a width of 2 μm, a length of 5 mm and consists of: (*i*) a 7 nm thick MgO layer that prevents the microwave current from flowing into the metal wedge, because this would create a complicated current distribution and an unpredictable magnetic field disturbing the CPW magnetic field; (*ii*) a 30 nm thick $Ni_{80}Fe_{20}$ layer that is excited externally by the CPW magnetic field and serves as a pumping layer for the attached metal wedge; (*iii*) an optional second 7 nm thick MgO interlayer to block spin pumping from the $Ni_{80}Fe_{20}$ layer into the metal wedge; (*iv*) a metal wedge composed of either silver, copper or platinum.

The optional MgO interlayer (*iii*) is used in a reference sample to separate the different contributions to the BLS intensity originating from the magnetic and the non-magnetic layer respectively. In the main sample without the MgO interlayer, spin pumping into the metal is expected to occur, whereas in the reference sample the pumping mechanism is blocked by the MgO layer. The latter is insulating but optically transparent, and therefore does not affect the detection by the probing laser

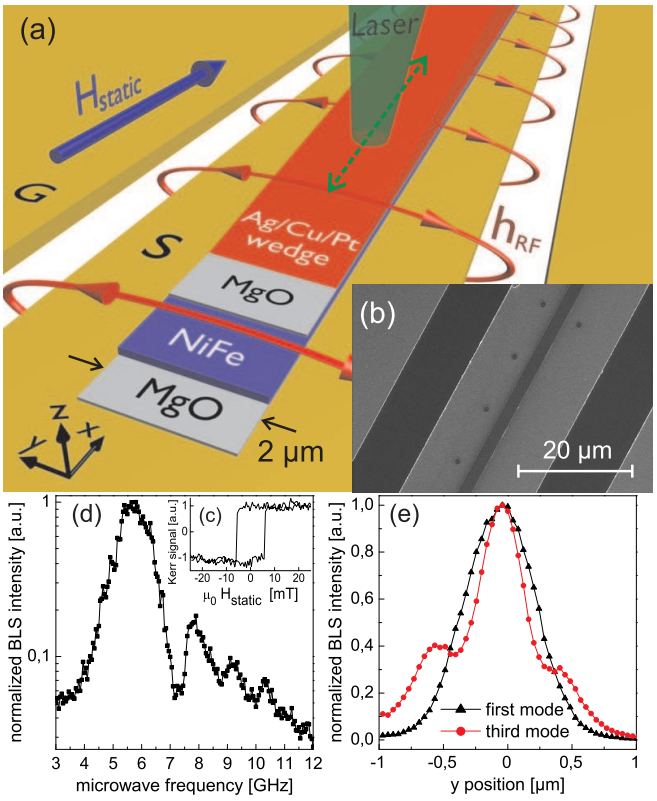

FIG. 1. (Color online) (a) Scheme of the sample layout and (b) SEM picture of the waveguide. A multilayer structure is prepared on top of a coplanar waveguide. A static magnetic field $\mu_0 H_{static}$ of 20 mT is applied parallel to the signal line and perpendicular to the dynamic magnetic field h_{RF}, which is caused by an alternating microwave current flowing through the coplanar waveguide. The magnetization in the $Ni_{80}Fe_{20}$ is excited by h_{RF} and spins are pumped into the metal wedge. (c) MOKE hysteresis loop to determine the saturation field in x-direction, (d) BLS spectrum taken on pure $Ni_{80}Fe_{20}$ at a static magnetic field of 20 mT. (e) BLS scans across the structure for the first two maxima of (d) at microwave frequencies of 5.5 GHz and 7.8 GHz. The profiles correspond to the first and the third laterally standing spin wave mode. The second mode is not excited.

light.

For absolut height calibration of the metal wedge, the scan position in x-direction is calculated into a total thickness. The topography was scanned in y-direction with a mechanical profilometer for different points along the wedge, and for each of these profiles the thickness of the multilayer was extracted with the CPW level as reference level.

Figure 1(d) shows the BLS spectrum taken on pure $Ni_{80}Fe_{20}$ at an applied field of 20 mT in x-direction. The first and most pronounced maximum is visible at a frequency of 5.5 GHz but several other maxima develop at higher frequencies corresponding to higher laterally standing spin wave modes across the stripe [15, 16].

A spatially uniform precession cannot be excited in a 2 μm wide stripe due to pinning effects at the boundaries. Standing spin waves build up across the width of the stripe in y-direction and the spin pumping efficiency becomes dependent on this direction (Fig. 1(e)). The dynamic magnetization in the non-magnetic layer experiences additional dephasing due to the mixing of components pumped with opposite initial phases from neighbouring antinodes of higher order standing waves. To minimize this contribution to the dephasing, only the first standing spin wave mode, excited at a microwave frequency of 5.5 GHz and an external field of 20 mT was used in our BLS measurements. The maximum of the first mode is located in the middle of the stripe and the BLS detection efficiency decreases with increasing metal wedge thickness on top of the $Ni_{80}Fe_{20}$ layer.

In Fig. 2 the measured BLS intensities of the maximum of the first mode are shown for different scan positions in x-direction. With increasing wedge thickness the BLS signal decays exponentially over a range of almost four decades in intensity. In the silver (Fig. 2(a)) and the copper wedge (Fig. 2(b)) the slopes of the exponential decay are different for the main (black dots) and the reference sample (red dots) whereas in the platinum sample both slopes are the same within the error bars (Fig. 2(c)).

The origin of the difference in silver and copper is the additional contribution to the BLS intensity due to the spin polarization pumped from the underlying $Ni_{80}Fe_{20}$ layer. While the BLS signal of the main sample is determined by the optical decay from the signal originating in $Ni_{80}Fe_{20}$ as well as by the decaying induced magnetization in copper, the signal from the sample with the MgO interlayer, which prevents spin pumping, contains only the signal originating from the $Ni_{80}Fe_{20}$ layer. In platinum this effect is not observable because the injected spin angular momentum is immediately transferred from the spin system to the lattice due to the high spin orbit interaction.

The total BLS intensity depends on the thickness of the metal wedge and consists of two contributions: One is due to the precessing magnetization in the ferromagnet, the other originates from the pumped spin polarization in the metal. The total BLS intensity is proportional to:

$$|E_F + E_N|^2 = |E_F|^2 + 2\,\mathrm{Re}\,(E_F E_N^*) + |E_N|^2 \qquad (1)$$

where E_F and E_N are the electric fields of the probe laser light scattered inelastically in the magnetic and the non-magnetic layer, respectively. Inside the metal wedge of thickness d, i.e. for $0 < z < d$, the profile of the electric field originating from the incident light can be expressed as a damped wave (see inset of Fig. 2).

$$E_F = E_{F,0} \exp\,(2i\tilde{n}kd) \qquad (2)$$

Here $\tilde{n} = n + i\kappa$ is the complex refractive index and $k = \omega/c$ is the vacuum wavevector of light. The factor

2 in the exponent takes into account that the BLS setup is prepared in backscattering geometry, and the light has to pass through the structure twice.

The amplitude of the backscattered light from the nonmagnetic layer is a sum of contributions originating from different depths of the wedge, weighted by the decaying probe laser amplitude as well as by the decaying contribution of the spin polarization to the scattered light.

$$E_{\mathrm{N}} = \int_0^d E_{\mathrm{N},0} \exp\left[2i\tilde{n}k\left(d-z\right)\right] \exp\left(-\frac{z}{l_2}\right) dz \qquad (3)$$

Here l_2 is the characteristic dephasing length of the dynamic spin polarization that gives rise to the BLS signal.

In Fig. 2 the fit curves (black and red lines) and the calculated BLS intensity for the pure spin part (blue line), obtained by a numerical simulation using Eqs. (1)-(3), are shown in addition to the measurement data. The fitting parameters in the simulation are the ratio of the field strengths $E_{\mathrm{N},0}$ and $E_{\mathrm{F},0}$ at the $Ni_{80}Fe_{20}$/Cu interface, the complex refractive index $\tilde{n}$ in the metal and the dephasing length l_2. The results of this simulation as well as the parameters of the fits in Fig. 2 are summarized in Tab. I. The contribution of the induced magnetization $|E_{\mathrm{N}}|^2$ to the BLS signal is at maximum for wedge thicknesses below 10 nm, even if the BLS signal originated from the $Ni_{80}Fe_{20}$ layer, $|E_{\mathrm{F}}|^2$ is dominant. Above wedge thicknesses of 20 nm in silver (45 nm in copper) $|E_{\mathrm{N}}|^2$ becomes dominating over $|E_{\mathrm{F}}|^2$.

With knowledge of l_2, a characteristic relaxation time T_2 can be calculated using wave-diffusion equations for the macroscopic spin density $\vec{\rho}_{\mathrm{s}}(z,t) = \vec{\rho}_{\uparrow}(z,t) - \vec{\rho}_{\downarrow}(z,t)$ and the spin-current density $\vec{J}_{\mathrm{s}}(z,t) = \vec{J}_{\uparrow}(z,t) - \vec{J}_{\downarrow}(z,t)$:

$$\frac{\partial \vec{\rho}_{\mathrm{s}}(z,t)}{\partial t} = -\gamma \vec{\rho}_{\mathrm{s}}(z,t) \times \vec{B} - \frac{\partial \vec{J}_{\mathrm{s}}(z,t)}{\partial z} - \frac{\partial \vec{\rho}_{\mathrm{s}}(z,t)}{\partial t}\bigg|_{\mathrm{int}}, \qquad (4)$$

and

$$\vec{J}_{\mathrm{s}}(z,t) = -D\frac{\partial \vec{\rho}_{\mathrm{s}}(z,t)}{\partial z} - \tau_{\mathrm{e}}\gamma \vec{J}_{\mathrm{s}}(z,t) \times \vec{B} - \tau_{\mathrm{e}}\frac{\partial \vec{J}_{\mathrm{s}}(z,t)}{\partial t}, \qquad (5)$$

Here, τ_{e} denotes the momentum relaxation time, γ is the absolute value of the electron ($g \approx 2$) gyromagnetic ratio, $\vec{B}$ is the magnetic field and D is the diffusion constant.

As a generalization of Ref. [17], we include different longitudinal (or spin-lattice) relaxation times T_1 and transverse (or spin-spin) relaxation times T_2 in the interaction contribution in Eq. (4): $\left(\partial \rho_{\mathrm{s}}(x)/\partial t\right)|_{\mathrm{int}} = \rho_{\mathrm{s}}(x)/T_1$ and $\left(\partial \rho_{\mathrm{s}}(y,z)/\partial t\right)|_{\mathrm{int}} = \rho_{\mathrm{s}}(y,z)/T_2$.

The dynamical components of $\vec{\rho}_{\mathrm{s}}(z,t)$ in Eq. (4) decay with T_2 and the static component decays with T_1. The latter is not accessible to Brillouin light scattering and is therefore neglected in the following.

It can be shown [17] that the relaxation times T_2 depend on the corresponding decay lengths l_2 via:

$$l_2 = \frac{v_{\mathrm{F}}}{\sqrt{3}}\sqrt{\tau_{\mathrm{e}} T_2} \qquad (6)$$

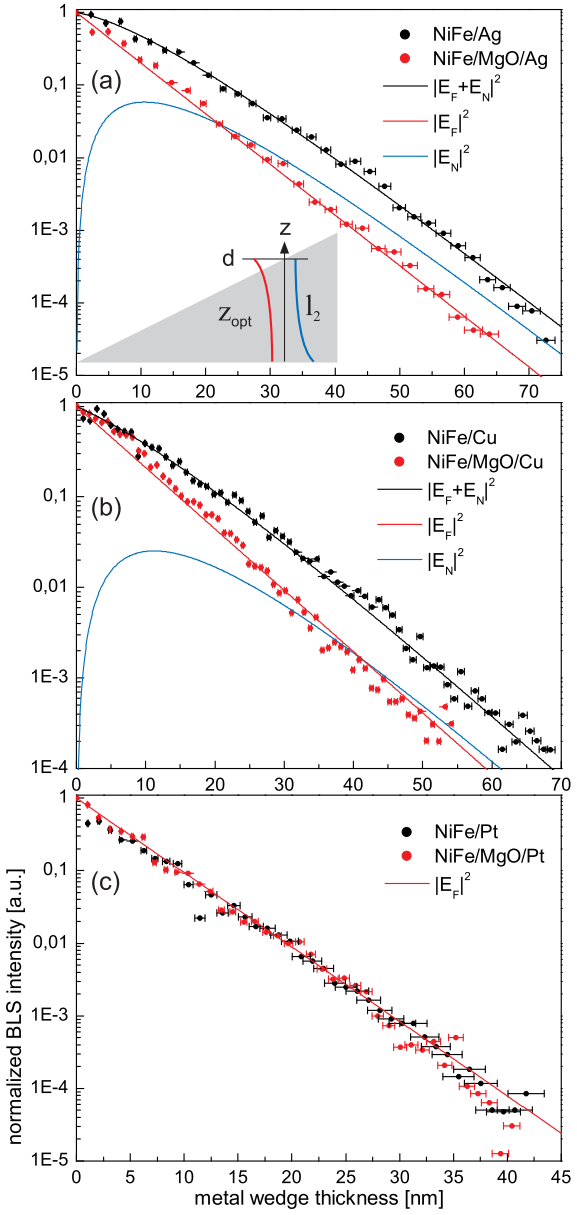

FIG. 2. (Color online) BLS scan data of the silver (a), the copper (b) and the platinum (c) wedged sample. Each graph shows the measurement of the main sample with active spin pumping (black dots) and the respective reference sample with blocked spin pumping (red dots). A difference between main and reference sample is only visible for silver and copper but not for platinum (see text). The error bars reflects the uncertainty in thickness determination by the mechanical profilometer. The black and red lines are fits of the scan data according to Eq. (1). The theoretical evolution of the pure spin part of the BLS signal (blue line) can be derived from the fitting parameters. The inset in (a) shows that the optical absorption length z_{opt} as well as the decay length of the transverse component l_2 contribute to the total BLS intensity probed by the laser over the entire thickness.

TABLE I. Fitting parameters of the BLS data in Fig. 2 and the resulting transverse relaxation time T_2 according to the macroscopic spin wave-equation.

Normal metal	$\tilde{n}$	$\tilde{n}_{\rm lit}$ in [18]	l_2 (nm)	$E_{\rm F,0}/E_{\rm N,0}$	T_2 (fs)
Ag	0.13+i3.4	0.13+i3.2	9 ±1	16	3 ±1
Cu	1.07+i3.3	1.07+i2.6	10 ±1	26	5 ±1
Pt	2.08+i5.2	2.08+i3.6	0 ±2	> 20	inst.

where $v_{\rm F}$ is the Fermi velocity.

To obtain the transverse relaxation time, we solve Eqs. (4) and (5) numerically by using T_2 as a fit parameter to match the experimentally determined value for l_2 (see Tab. I). According to Ref. [19] we use $\tau_{\rm e}\,({\rm Cu}) = 25\,{\rm fs}$ and $\tau_{\rm e}\,({\rm Ag}) = 40\,{\rm fs}$ for the momentum relaxation time and $v_{\rm F}\,({\rm Cu}) = 1.57\,{\rm nm/fs}$ and $v_{\rm F}\,({\rm Ag}) = 1.39\,{\rm nm/fs}$ for the Fermi velocity at room temperature. The influence of the small external magnetic field of 20 mT and the injection frequency of 5.5 GHz on the decay lengths is negligible in the calculations. This result is also confirmed by our BLS measurements of the copper sample: The decay is unchanged within the error bars at an injection frequency of 9.3 GHz and an applied field of 70 mT.

Note that the accepted value of the longitudinal relaxation time T_1, of a few picoseconds [20, 21], exceeds the value of T_2 determined by our BLS measurements by three orders of magnitude. This is remarkable because T_2 is usually considered equivalent to T_1, if the mean electron scattering time $\tau_{\rm e}$ is much smaller than the reciprocal Larmor frequency [22].

We do not rule out an intrinsic difference between T_1 and T_2, but the magnitude of the discrepancy suggests an extrinsic effect acting differently on the transverse and the longitudinal component of the induced magnetization. We assume a non-homogeneous $Ni_{80}Fe_{20}$/metal interface due to residual mass diffusion of nickel and iron atoms from the $Ni_{80}Fe_{20}$ layer into defects of the normal metal. The induced magnetization will give rise to a spin torque, i.e. the transverse component of the pumped spin current is effectively absorbed on a short length scale as shown theoretically in [23] for the case of a spin current transmitted from a nonmagnet into a ferromagnet. In our case this ferromagnet is replaced by the paramagnetic impurities and the transverse spin current is limited to a few nanometers. The longitudinal component of the induced magnetization will not be affected by the impurities.

In conclusion we have determined for the first time the existence of magnetization in non-magnetic metals by optical means. We have also shown that the transverse magnetization component is directly accessible to Brillouin light scattering microscopy and may decay faster in the non-magnetic material than usually assumed. The result confirms that a high purity of the interface is essential for an efficient transmission of the transverse spin current from the ferromagnet to the non-magnetic metal.

Support by the Deutsche Forschungsgemeinschaft and the Japan Science and Technology Agency within the project JST-DFG Hi380/21-1 is gratefully acknowledged.

* current address: Department of Physics, VSB - Technical University of Ostrava, 708 33 Ostrava, Czech Republic.
† current address: Materials Science Division and Center for Nanoscale Materials, Argonne National Laboratory, Argonne, Illinois 60439, USA.

[1] G.A. Prinz, Science **282**, 1660 (1998).
[2] S.A. Wolf et al., Science **294**, 1488 (2001).
[3] M. Johnson, Phys. Rev. Lett.**70**, 2142 (1993).
[4] J.E. Hirsch, Phys. Rev. Lett.**83**, 1834 (1999).
[5] R.H. Silsbee, A. Janossy, P. Monod, Phys. Rev. B**19**, 4382 (1979).
[6] Y. Tserkovnyak, A. Brataas, G.E. Bauer, Phys. Rev. Lett.**88**, 11 (2002).
[7] T. Gerrits, M.L. Schneider, T.J. Silva, J. Appl. Phys. **99**, 023901 (2006).
[8] F.J. Jedema, A.T. Filip, B.J. van Wees, Nature **410**, 345 (2001).
[9] T. Kimura, J. Hamrle, Y. Otani, K. Tsukagoshi, Y. Aoyagi , Appl. Phys. Lett.**85**, 3501 (2004).
[10] S.O. Valenzuela, M. Tinkham, Nature **442**, 176 (2006).
[11] E. Saitoh, M. Ueda, H. Miyajima, Appl. Phys. Lett.**88**, 182509 (2006).
[12] T. Kimura, Y. Otani, T. Sato, S. Takahashi, S. Maekawa, Phys. Rev. Lett.**98**, 156601 (2007).
[13] S.A. Crooker, M. Furis, X. Lou, C. Adelmann, D.L. Smith, C.J. Palmstrøm, P.A. Crowell, Science **309**, 2191 (2005).
[14] O. Mosendz, G. Mihajlovic, J.E. Pearson, P. Fischer, M.Y. Im, S.D. Bader, A. Hoffmann, Phys. Rev. B**80**, 104439 (2009).
[15] S.O. Demokritov, B. Hillebrands, and A.N. Slavin, Phys. Rep. **348**, 441 (2001).
[16] C. Bayer et al. Phys. Rev. B**72**, 064427 (2005).
[17] Y. Zhu, B. Hillebrands, and H.C. Schneider, Phys. Rev. B**79**, 214412 (2009).
[18] E.D. Palik, Handbook of Optical Constants of Solids, Academic Press, Boston (1985).
[19] N.W. Ashcroft, N.D. Mermin, Solid State Phyics, Holt, Rinehart and Winston, New York (1976)
[20] J. Bass, W.P. Pratt Jr., J. Phys.: Condens. Matter **19**, 183201 (2007).
[21] F.J. Jedema, M.S. Nijboer, A.T. Filip, and B.J. van Wees, Phys. Rev. B**67**, 085319 (2003).
[22] D. Pines, C.P. Slichter, Phys. Rev. **100**, 1014 (1955).
[23] M.D. Stiles, A. Zangwill, Phys. Rev. B**66**, 014407 (2002).